

Evanescient Optothermoelectric Trapping: Deeper Potentials at a Largescale

Chaudhary Eksha Rani, Rahul Chand, Ashutosh Shukla, and G V Pavan Kumar*

*Department of Physics, Indian Institute of Science Education and Research (IISER) Pune,
Pune 411008, India*

E-mail: pavan@iiserpune.ac.in

Abstract

Surface plasmons (SP) and their mediated effects have been widely used to manipulate micro- and nanoscale objects of dielectric and metallic nature. In this work, we show how SP excitation can be used to induce thermofluidic and thermoelectric effects to manipulate colloidal dynamics on a large scale. In an evanescent plasmonic trap, temperature gradients induce fluid flow that can facilitate particle accumulation. However, large out-of-plane flows expel particles from the trap, resulting in a shallow trap potential. Here, we numerically demonstrate how adding thermoelectric fields can overpower the optical and hydrodynamic forces to achieve a stable nanoparticle assembly at low excitation powers. We calculate the corresponding optical, fluidic, and thermoelectric trapping forces and potentials. These potentials can be enabled without resonant SP excitation, which requires careful optical alignment. Thus, we explain the mechanism of how, despite weak optical intensities and forces, sufficient trapping force can be supplied via the evanescent optothermoelectric trap to obtain large-scale reversible nanoparticle assemblies, irrespective of their shape, size, or material.

Introduction

Trapping and tweezing of Brownian objects received impetus thanks to the pioneering work of Ashkin and coworkers.¹⁻⁵ The initial and subsequent optical tweezer designs use high numerical aperture objective lenses to spatiotemporally trap and move micro- and nanoscopic objects.⁶⁻¹¹ In certain applications like microfluidics, biomedicine, and optically driven soft and active matter large-area spatiotemporal traps are required. This has motivated research on ‘macro’ optical traps extending up to a few millimetres. One way to do this is to utilize evanescent waves from the total internal reflection (TIR) of a laser that can confine objects to an area defined by the projected evanescent waves.¹²⁻¹⁵ However, creating such large-area optical traps is a challenge. They require large powers of hundreds of milliwatts, multiple laser channels in case of counterpropagating evanescent waves, and careful optical alignment, making them difficult to deploy in power-sensitive environments such as cell manipulation. Additionally, since optical forces are not long-ranged, these traps rely on particle diffusion, making them time-intensive.¹⁶

An alternate strategy is to utilize these evanescent waves to excite surface plasmons (SP),¹⁷ facilitating radiative and absorptive channels for energy exchange that lead to opto-thermal potentials.¹⁸⁻²² Our group has developed large-area optothermal trapping and tweezing methods that can be harnessed for single-molecule spectroscopy and dynamic lithography.^{23,24} However, these traps depend on the size, shape, and material of the particle, making them highly selective.²³ These trapping methods are also extremely sensitive to the plasmonic resonances of the metal, which requires tuning the incident wavelength,²⁵ and polarisation.²⁶ Moreover, SP need to be excited resonantly at the surface plasmon resonance (SPR) angle to maximize the optical forces, which requires additional experimental equipment and optical alignment.^{27,28} An unavoidable consequence of SP excitation is the large temperature gradients, which induce strong fluid flows that can make the trap unstable. It is imperative to develop optical trapping mechanisms that utilise the consequent effects of heat and fluid

flow while relaxing the resonant excitation conditions to achieve large-scale, stable traps.^{29–34} Here, we demonstrate one such mechanism using the opto-thermoelectric (OTE) effect, which enables large-scale reversible trapping using low power non-resonant optical excitation irrespective of the particle characteristics.^{35–40} While most OTE-based trapping studies have focused on small-area traps, a systematic study on large-area OTE traps is necessary.

In this article, we present our numerical study of evanescent OTE traps that unveil the relative contributions of optical, hydrodynamic, and OTE fields, showing a boost in trapping forces when OTE is employed. Consider the geometry as shown in Figure 1(a), consisting of the glass and water domains with a 50 nm thin film of gold (Au) sandwiched in between. Gold nanoparticles (AuNP) of diameter $2r = 400$ nm, 200 nm, 300 nm, or 100 nm are considered diffusing in water. SP are evanescently excited in the Au film that exert negligible optical force. SP also lead to a temperature hotspot in the excitation region that induces a fluid flow directed towards the hotspot. The in-plane flows exert strong hydrodynamic forces to assemble AuNPs, but the out-of-plane flow tends to make the thermofluidic trap unstable. To stabilize the trap, we introduce a thermoelectric field by considering the presence of ions in the fluid, which migrate under a temperature gradient. Since the thermoelectric field is generated by optically-created temperatures, the resultant force is called optothermoelectric force. It overpowers the thermofluidic trapping forces by multiple orders of magnitude and enables a stable assembly of AuNPs. Finite element method-based simulations in COMSOL multiphysics are used to compute the plasmonic optical fields, temperature distribution, optothermally induced fluid flow, and thermoelectric fields. The corresponding forces and potentials experienced by an AuNP are calculated to explain the relative role played by each. The material parameters considered are directly taken from the in-built material library of COMSOL multiphysics unless mentioned otherwise.

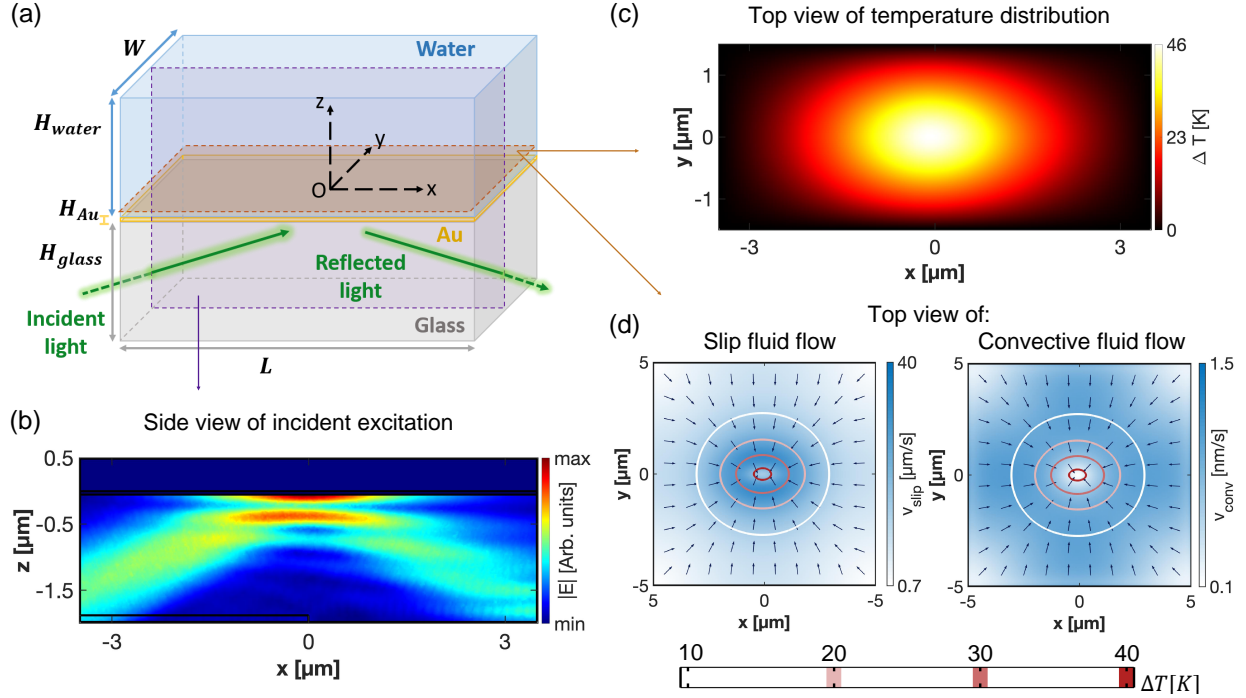


Figure 1: (a) Geometry simulated to compute the fields. (b) XZ profile of Gaussian wave exhibiting TIR at an angle $\theta_i = 67^\circ$, greater than the glass-water critical angle $\theta_c = 66.5^\circ$. (c) XY profile of elliptical temperature distribution on the Au film (thermal conductivity 150 W/m.K) due to SP excitation. (d) Laser heating induced slip and convective fluid flows in the XY plane 100 nm above Au film in an enlarged geometry.

Model and theory

Electromagnetic field: Figure 1 (a) shows the Kretschmann configuration used to excite surface plasmons in the gold film.²³ A p-polarised Gaussian electromagnetic wave is incident on the glass-water interface at an angle $\theta_i = 67^\circ$, such that it undergoes total internal reflection (critical angle $\theta_c \sim 66.5^\circ$). Consequently, evanescent waves are generated in the water (rarer) medium, which can excite SP in the metal film. The SP intensity can be controlled by changing the incident power or polarisation⁴¹ since only the TM electromagnetic wave can excite SPs in this configuration. The electromagnetic field is simulated using the ‘electromagnetic wave frequency domain’ (*ewfd*) module. Being computationally expensive, *ewfd* limits the maximum geometrical dimension that can be simulated. Employing scattering boundary conditions, the geometric dimensions are carefully chosen to avoid any boundary

reflections from the reflected wave: $H_{water} = 0.5 \mu\text{m}$, $H_{glass} = 2 \mu\text{m}$, $L = 7 \mu\text{m}$, $W = 3 \mu\text{m}$. The XZ profile of the incident light (p-polarised, $\lambda = 532 \text{ nm}$, power 10 mW) undergoing TIR is shown in Figure 1(b), which gives surface fields at the Au-water interface. It should be mentioned that such surface fields are not observed when s-polarized incident light is simulated, which confirms the SP excitation.

Thermofluidic field: SP generation in the metal film leads to energy dissipation via the Joule effect.⁴² In the temperature homogenization regime, the temperature distribution will directly correspond with the intensity distribution. An obliquely incident Gaussian beam will result in an elliptical intensity spot⁴³ which corresponds to an elliptical temperature distribution on the Au surface, as shown in Figure 1(c). The temperature magnitude can be controlled using the SP intensity by tuning the power or polarization of the incident light. Ideally, s-polarised light will not lead to any temperature rise due to its inability to excite SP. The SP-mediated heat is modeled in COMSOL using the ‘heat transfer in solids and fluids’ (*ht*) module coupled with the *ewfd* module.

The heated Au film leads to temperature-induced fluid flows of two types: (1) convective fluid flow arising from temperature-dependent density of water and (2) slip fluid flow arising from temperature-dependent interfacial interactions.⁴⁴ These fluid flows are simulated using the ‘laminar flow’ (*spf*) module coupled to the *ht* module. The Au-water interface is set to slip boundary condition with a dimensionless slip coefficient $\sigma_T = 0.001$ ⁴⁵ to compute the slip flow and no-slip boundary condition to compute the convective flow. All other walls are set to open boundary conditions. However, experiments with colloidal solutions are usually performed in larger fluid columns to minimize boundary effects on colloidal diffusion. But, since computing such large domains is extremely memory-expensive for *ewfd*, we used an alternative heat source called ‘deposited beam power’ that models the temperature profile of a laser-heated surface without explicitly modeling the laser. Thus, eliminating *ewfd*, we enlarged the fluid column while significantly reducing the computational resources needed:

$H_{water} = 5 \mu\text{m}$, $H_{glass} = 2 \mu\text{m}$, $L = 10 \mu\text{m}$, $W = 10 \mu\text{m}$. The parameters of the Gaussian laser used by ‘deposited beam power’ are carefully chosen to match the temperature profile generated via the *ewfd*-mediated heat source. The corresponding slip and convective fluid flow in the XY plane (100 nm above Au surface) are shown in Figure 1(d), where the contours represent the temperature rise against a room temperature of 298 K.

Thermoelectric field: If the fluid contains ions that migrate differently under a temperature gradient, then spatial separation of ions can be achieved.^{40,46} This will produce an electrostatic field in the fluid called the thermoelectric field $E_T = \frac{k_B T \nabla T}{e} \frac{\sum_i Z_i c_i S_{T_i}}{\sum_i Z_i^2 c_i}$, directed along the temperature gradient. Here, i indicates the ionic species, k_B is the Boltzmann constant, e is the elementary charge, Z is the charge number, and c is the concentration of ions. Once E_T is activated, it can exert thermoelectric force $F^{OTE} = Q \cdot E_T$ on any particle having total charge Q , driving it towards or away from the hotspot. The temperature T and its gradient ∇T are extracted from the COMSOL model to compute the thermoelectric fields and forces.

Results and discussion

Optical force: A spherical AuNP is modeled in the water domain 20 nm above the Au surface (which is of the order of Debye length)^{43,47,48} at the center of the SP excitation spot. The optical forces exerted due to SP fields are calculated by integrating the Maxwell stress tensor over the AuNP surface.⁴⁹ The resultant optical forces are of the order $10^{-22} - 10^{-20}$ N, which is negligibly small compared to the Brownian forces experienced by these particles in the range $10^{-16} - 10^{-14}$ N.²⁵ Such weak optical forces are due to the non-resonant excitation of SP at θ_i , where only a small fraction of incident power is coupled to SP, and the majority is reflected back into glass. To maximize the optical forces up to a femtonewton order, (1) SP can be resonantly excited at SPR angle well beyond θ_c ,^{27,28} or (2) laser power

can be increased,²⁷ or (3) particle resonances can be matched with the laser wavelength²⁵ and polarization.^{23,50} Experimentally, it may not always be possible to tune θ_i to the SPR angle or optimize the trap to match particle resonances. Moreover, largescale trapping will require large input powers. To execute an efficient trap without changing the excitation angle, power, or wavelength, it is imperative to utilize the dissipated optical energy in the form of heat to manipulate colloids. Given the small magnitude of optical forces, we consider that the SP fields have minimal effect on particle dynamics.

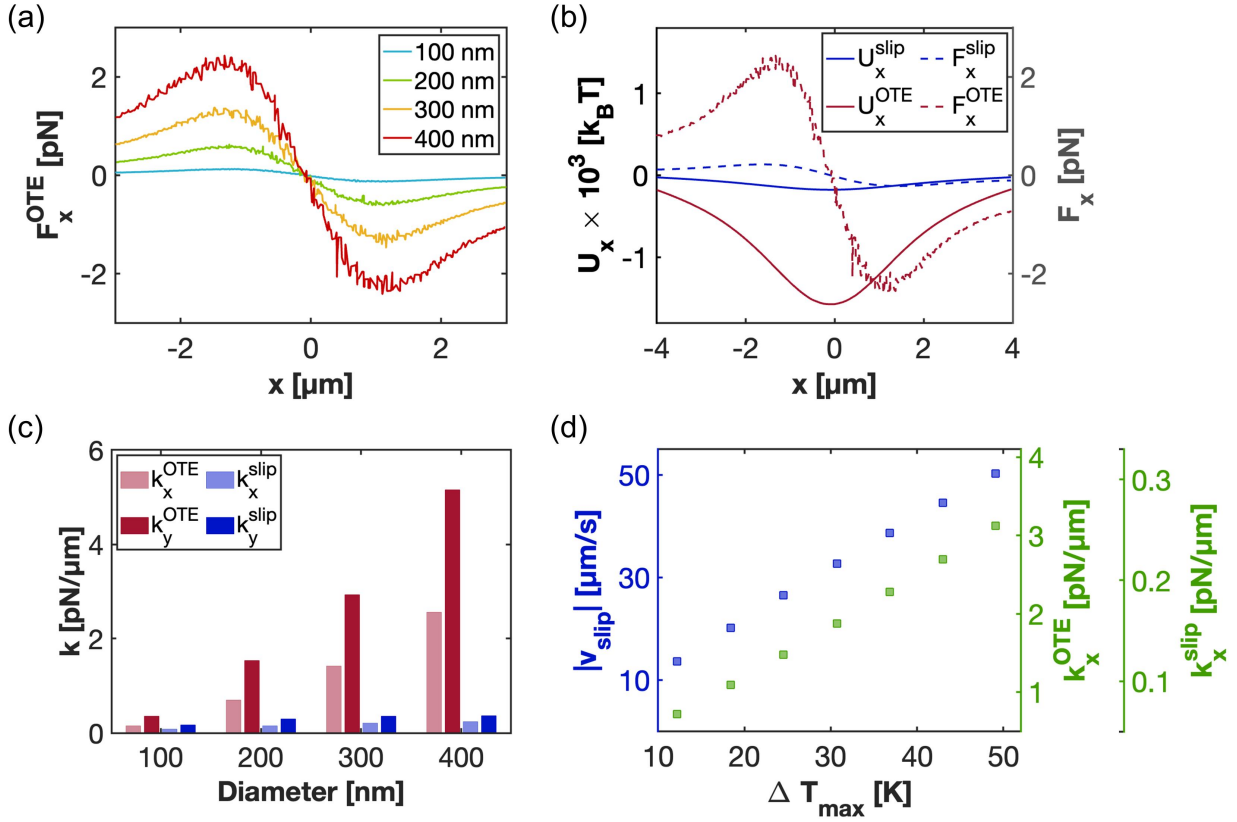


Figure 2: (a) x-component of thermoelectric force F_x^{OTE} exerted on AuNPs of different diameters. (b) Comparison between trap potential U_x felt by a 400 nm AuNP along X due to OTE and slip forces. (c) Comparison between the trap stiffness (k) along X and Y due to $F_{x,y}^{OTE}$ and $F_{x,y}^{slip}$ forces for AuNP of different diameters. (d) Variation of maximum slip flow velocity and trap stiffness for 400 nm AuNP, due to F_x^{OTE} and F_x^{slip} forces, with maximum temperature rise ΔT_{max} .

OTE and hydrodynamic slip force calculation: The most prominent heat-mediated ef-

facts widely used in trapping are the thermophoresis,³¹ thermofluidic⁵¹ and thermoelectric³⁵ effects. Since metallic colloids do not exhibit thermophoresis, AuNP does not migrate under a temperature gradient⁴⁴ and will be driven by the fluid flow in the system under the effect of hydrodynamic forces. We have done a numerical study to compare the two remaining effects and found that the thermoelectric force is much stronger and gives greater control over particle dynamics than the thermofluidic forces. To study the thermoelectric effect, consider an AuNP freely diffusing in a 5 mM solution of a surfactant CTAC (cetyltrimethylammonium chloride) that dissociates into CTA⁺ and Cl⁻ ions. Above the critical micellar concentration, CTAC self-assembles into micelles, forming macrocations. The CTAC molecules get adsorbed on the AuNP surface, forming a double layer and making it positively charged with a zeta potential ζ . We have approximated $\zeta = 63.6$ mV, 73.3 mV, 76 mV, and 80 mV for $2r = 100$ nm, 200 nm, 300 nm, and 400 nm, respectively,⁵² considering the general trend of ζ measurements in 5 mM CTAC. Without a temperature gradient, the positively charged AuNP, CTAC micelles, and Cl⁻ ions are randomly dispersed in the solution. Under the SP-mediated temperature gradient, the micelles and Cl⁻ ions will move differently owing to their different Soret coefficients (CTAC micelles: 10^{-2} , Cl⁻ ions: 7.18×10^{-4}),⁵³ leading to a spatial separation between positive and negative ions. This generates an electrostatic field E_T that can exert thermoelectric force $F^{OTE} = (4\pi r^2 \sigma) \cdot E_T$ on a spherical particle having surface charge density σ .⁵⁴ Using $T\nabla T$ from the COMSOL simulation, we computed the force components F_x^{OTE} , F_y^{OTE} , and F_z^{OTE} exerted on an AuNP located 20 nm above the Au surface. F_x^{OTE} , shown in Figure 2(a), in the pN order, is much stronger than the minimum fN order of trapping force required to confine AuNP at the hotspot. The magnitude and slope increase with particle size $2r$ due to the greater zeta potential of larger particles, giving them greater surface charge.

To compare with the thermofluidic effects, we estimated the hydrodynamic force on AuNP due to temperature-induced fluid flows. For a spherical particle with a small Reynolds num-

ber ($\sim 10^{-6}$), the hydrodynamic force is given by the Stokes equation $F = \gamma \cdot v = 6\pi\eta rv$, where η is the dynamic viscosity of the fluid, v is the fluid velocity, and γ is the friction coefficient near a surface, which gets modified compared to its bulk value γ_0 as $\gamma = \alpha\gamma_0$.^{49,55} Using the slip or convective flow velocity from COMSOL, we can calculate the hydrodynamic slip and convective forces, F^{slip} and F^{conv} , respectively.

OTE vs hydrodynamic force: To compare the OTE and the fluid forces, we will consider the 400 nm AuNP. Figure 2(b) shows the x-component of OTE, F_x^{OTE} , and hydrodynamic slip forces F_x^{slip} , along with the respective potentials U_x . We consider only F_x^{slip} for comparison as it is larger of the two fluid forces. While both F_x^{OTE} and F_x^{slip} are strong enough to trap AuNPs, F_x^{OTE} is ten times stronger with a thermoelectric trap stiffness $k_x^{OTE} = 2.56$ pN/ μ m compared to the thermofluidic trap stiffness $k_x^{slip} = 0.24$ pN/ μ m. This results in a thermoelectric potential U_x^{OTE} that is over eight times deeper than the thermofluidic potential U_x^{slip} , trapping the AuNP in the surface plane above the hotspot. Due to the elliptical shape of the temperature distribution, as is evident from the contours in Figure 1(d), the temperature gradients along Y are greater than those along X. This results in steeper force profiles and a larger trap stiffness along Y, $k_y \sim 2k_x$, for both OTE and hydrodynamic slip forces as is shown in Figure 2(c). Thus, AuNP diffusing in water will be driven toward the hotspot collectively by $F_{x,y}^{OTE}$ and $F_{x,y}^{slip}$ (in-plane forces), which facilitate an elliptical region of closely assembled AuNP above the hotspot. It should be emphasized that temperature is the primary control parameter for both thermofluidic and thermoelectric traps, as depicted by Figure 2(d) (for the 400 nm AuNP). The maximum slip velocity v_{slip} varies linearly with ΔT_{max} due to its dependence on temperature as $\vec{v}_{slip} = \chi \nabla T / T$,⁴⁴ directly affecting the thermofluidic trap stiffness k_x^{slip} , where, χ is the thermo-osmotic slip coefficient. The rising temperature will also strengthen E_T , leading to a stronger F^{OTE} and increasing k_x^{OTE} . Figure 2(d) also shows that k_x^{slip} is one order of magnitude smaller than its thermoelectric counterpart k_x^{OTE} . The y-components of the forces and potentials exhibit a similar trend as

the x-components but with steeper force profiles and deeper potentials. Note that, up to an extent, F^{OTE} can be increased while keeping F^{slip} constant by increasing the CTAC concentration, enhancing E_T and thus the forces. However, to calculate the precise enhancement, we require zeta potential of AuNP in the increased concentration. For further comparison, we will continue the analysis considering 5 mM concentration of CTAC.

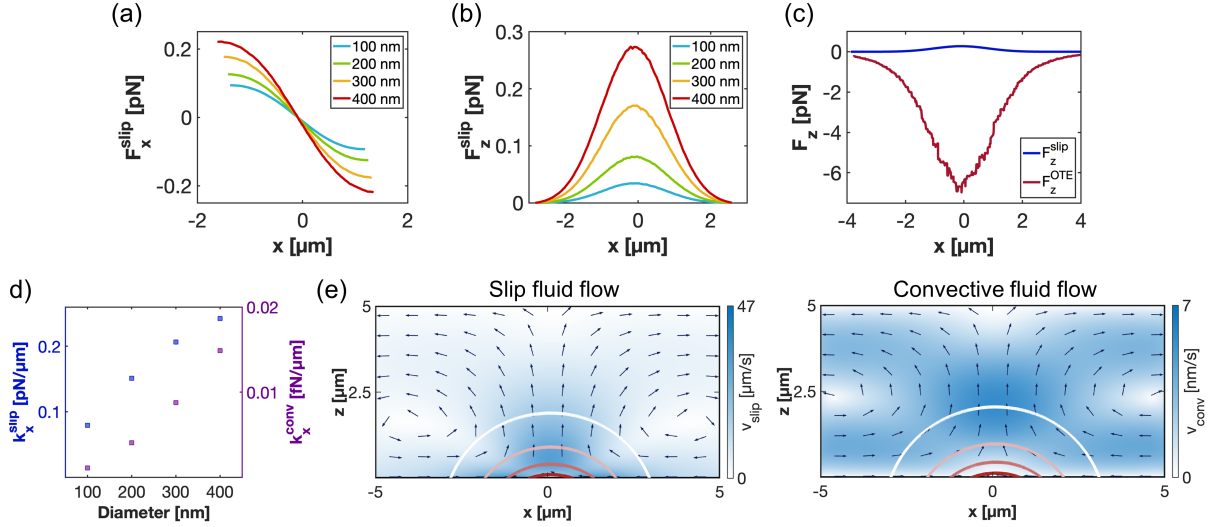


Figure 3: Hydrodynamic forces: (a) and (b) represent the F_x^{slip} and F_z^{slip} forces on AuNP of different diameters. (c) Comparison between F_z^{slip} and F_z^{OTE} forces showing their opposing nature. (d) Variation of trap stiffness with AuNP diameter due to hydrodynamic slip and convective forces. (e) XZ profile of slip and convective fluid flow, along with contours showing temperature rise.

Optical field enhancement: SP, being evanescent fields, decay exponentially away from the Au surface, which is why certain applications like biosensing and Raman spectroscopy require the objects to be very close to the surface. But, temperature-induced fluid flows like slip flow can pose a challenge. The x- and z-components of hydrodynamic slip forces, F_x^{slip} and F_z^{slip} , on an AuNP located 20 nm above the surface are shown in Figures 3(a) and 3(b), respectively. An increase in forces with particle size is expected due to the smaller diffusion coefficient of larger particles and the dependence of hydrodynamic forces on particle size. These sub-pN F^{slip} forces are sufficient to influence the Brownian dynamics of the AuNP

and result in a strong enough thermofluidic trap that can assemble AuNP above the hotspot. However, the assembled AuNP are unable to interact with the evanescent SP field due to the slightly stronger out-of-plane force F_z^{slip} , which expels the AuNP out of the trap volume. This makes the trap unstable in the vertical dimension. The instability is countered by the negative F_z^{OTE} , as plotted in Figure 3(c), which is directed towards the hotspot. It is seven times stronger than the positive F_z^{slip} , effectively opposing the upward pull and enabling a stable trap in the vertical dimension. Being closely confined to the surface, the particles can interact with the evanescent SP fields and create subwavelength gaps where the electric field can be localized and enhanced by multiple orders. Such confinement is crucial for applications like plasmonic sensing⁵⁶ and multiple scattering experiments like lasing from colloidal assemblies.⁵⁷ Inferring from Figure 2(d), large temperatures will tend to strengthen F_z^{slip} fluidic forces, making the trap unstable at large powers. But, in the presence of ions, the temperatures will also reinforce the thermoelectric field and F_z^{OTE} will facilitate stable trapping close to the surface. Hence, evanescent-OTE trap facilitates stable potential at both low powers, when thermofluidic potentials are shallow, and at high powers, when thermofluidic traps are unstable.

Hydrodynamic convective forces: Hydrodynamic convective forces F^{conv} are calculated using the convective flow velocity v_{conv} and are in the order $10^{-2} - 10^{-3}$ fN. Figure 3(d) compares the trap stiffness due to F_x^{conv} and F_x^{slip} for different sizes of AuNP. While both k_x^{conv} and k_x^{slip} increase with particle size, k_x^{conv} shows a concave-up increase and k_x^{slip} a concave-down increase. This can be understood from the dependence of the hydrodynamic force on γ and v . As the particle size increases, its center-to-surface distance increases and γ increases for both kinds of flows. However, from Figure 3(e), two distinct characteristics of v can be observed: (1) v_{slip} is three orders of magnitude stronger than v_{conv} , and (2) v_{slip} is stronger near the interface while v_{conv} is stronger in the bulk fluid, that is, v_{slip} decreases while v_{conv} increases as we go higher in z . This results in a steeper increase in k_x^{conv} compared to a flatter

rise in k_x^{slip} . Despite such trends, the slip forces result in a much stiffer trap, exceeding the trap stiffness due to convective forces by at least four orders of magnitude. From this, we can disregard the effect of convective fluid flow on AuNP dynamics. Additionally, for smaller fluid columns like the one considered here, the convective fluid flows are largely suppressed, and slip fluid flow dominates the particle dynamics.

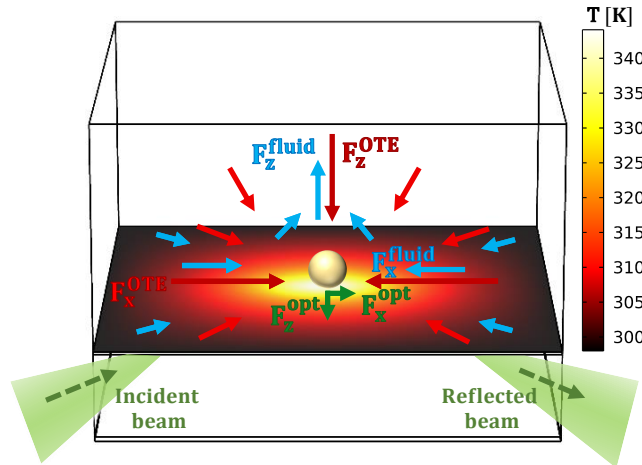


Figure 4: Schematic representing the different forces acting on an AuNP suspended above an evanescently excited Au film.

Control parameters of the trap: A schematic of the resultant forces is shown in Figure 4, depicting the respective forces acting in the system, mediated by the temperature rise from laser heating in an evanescent-O TE trap. The primary control parameter of both hydrodynamic and thermoelectric forces is the temperature distribution, which depends on the SP intensity. Besides varying SP intensity directly from the laser power, the polarization can be switched between p- and s- to control the fraction of incident light converted to SP. Also, illuminating at SPR angle can induce large temperature rise even at small laser powers. The trap will vanish instantaneously upon the removal of temperature gradients, making the assembly formation a reversible process. Loosely focusing the laser at an oblique angle provides large-scale illumination and temperature gradients over a large area, which dictates the assembly dimension. Once the trap begins to form, the accumulated AuNP will interact

with the SP fields, leading to intensity enhancement. This will heat the AuNP, acting as positive feedback that enhances the hydrodynamic and thermoelectric effects. Moreover, thermoelectric forces can additionally be controlled by the ionic concentration, given the direct dependence of the thermoelectric field on concentration.

Conclusion

We have demonstrated the working mechanism of an evanescent-optothermoelectric trap that can reversibly assemble metallic nanoparticles of any shape or material on a large scale, with particle radius down to 50 nm. While the simulations depict results for a smaller dimension, the same can be extended to a larger scale to obtain similar results. Large-scale TIR-illumination can access a large working area spanning hundreds of microns without using complex experimental optics or delicate fabricated structures, giving large-scale trap potentials. The potential depth depends on the temperature magnitude generated due to the illumination and ionic concentration. The temperature magnitude is controlled by incident power, polarization, and excitation angle. Since optical forces are not the major player, the trap is independent of particle characteristics and requires no resonance matching, wavelength tuning, high NA lens, or high powers. While optically mediated hydrodynamic forces lead to a thermofluidic trap, it is unstable in the vertical dimension. Whereas, thermoelectric forces can be 10 times stronger than hydrodynamic forces and facilitate deeper potentials to trap and assemble nanoparticles close to the surface. Such closely assembled particles can achieve excellent electric field enhancement, having direct applications in SERS.²³ Careful tuning of F^{OTE} and F^{slip} can result in applications like particle sorting without the need for multiple lasers.²⁵ Importantly, the large illumination area (\sim sub-mm) results in very small intensities (tens of mW in hundreds of μm^2), yet enough to assemble nanoparticles on such a large scale,²⁴ compared to $0.1 \text{ mW}/\mu\text{m}^2$ used to assemble over a few microns.⁵³ Once the assembly is formed, particles can self-heat, sustaining the trap even without metal film. Such

an assembly can potentially be transferred as a single entity.⁵⁶ Moreover, dielectric particles can be trapped using this method despite their thermophobic behavior.²⁷ We anticipate large-area traps to be useful in dynamic lithography of small entities such as Brownian colloids and bio-macromolecules. The strategy can also confine larger biological entities such as cells. This expands the capability of evanescent optical trapping from molecular to cellular scale without incrementing laser powers.

Acknowledgement

The authors thank Dr. Sunny Tiwari, Dr. Diptabrata Paul, and Dr. Shailendra Kumar Chaubey for valuable discussions related to this project. This work was partially funded by AOARD (grant number FA2386-23-1-4054) and the Swarnajayanti fellowship grant (DST/SJF/PSA-02/2017-18) to GVPK.

References

- (1) Ashkin, A. Acceleration and trapping of particles by radiation pressure. *Physical Review Letters* **1970**, *24*, 156.
- (2) Ashkin, A.; Dziedzic, J. M.; Bjorkholm, J. E.; Chu, S. Observation of a Single-Beam Gradient Force Optical Trap for Dielectric Particles. *Optics Letters* **1986**, *11*, 288–290.
- (3) Ashkin, A.; Dziedzic, J. M. Optical Trapping and Manipulation of Viruses and Bacteria. *Science* **1987**, *235*, 1517–1520.
- (4) Ashkin, A.; Dziedzic, J. M.; Yamane, T. Optical trapping and manipulation of single cells using infrared laser beams. *Nature* **1987**, *330*, 769–771.
- (5) Šiler, M.; Čižmár, T.; Šerý, M.; Zemánek, P. Optical forces generated by evanescent

- standing waves and their usage for sub-micron particle delivery. *Applied Physics B* **2006**, *84*, 157–165.
- (6) Grier, D. G. A Revolution in Optical Manipulation. *Nature* **2003**, *424*, 810–816.
- (7) Bradac, C. Nanoscale Optical Trapping: A Review. *Advanced Optical Materials* **2018**, *6*, 1800005.
- (8) Crozier, K. B. Quo Vadis, Plasmonic Optical Tweezers? *Light: Science & Applications* **2019**, *8*, 35.
- (9) Volpe, G. et al. Roadmap for Optical Tweezers. *Journal of Physics: Photonics* **2023**, *5*, 022501.
- (10) Nalupurackal, G.; Murugan, G.; Lokesh, M.; Vaippully, R.; Chauhan, A.; Nanda, B. R. K.; Sudakar, C.; Kotamarthi, H. C.; Datta, P.; Sinha Mahapatra, P.; others Simultaneous optical trapping and electromagnetic micromanipulation of ferromagnetically doped nayf4 microparticles. *ACS Applied Optical Materials* **2023**, *1*, 615–622.
- (11) Panja, K.; Goswami, J.; Nalupurackal, G.; Chakraborty, S.; Roy, S.; Roy, B.; Singh, R. Nonlinear dynamics of a microparticle in a hydro-thermophoretic trap. *Results in Physics* **2024**, *61*, 107709.
- (12) Righini, M.; Girard, C.; Quidant, R. Light-Induced Manipulation with Surface Plasmons. *Journal of Optics A: Pure and Applied Optics* **2008**, *10*, 093001.
- (13) Yoon, Y.-Z.; Cicuta, P. Optical Trapping of Colloidal Particles and Cells by Focused Evanescent Fields Using Conical Lenses. *Optics Express* **2010**, *18*, 7076–7084.
- (14) Yu, X.; Torisawa, T.; Umeda, N. Manipulation of particles with counter-propagating evanescent waves. *Chinese Physics Letters* **2007**, *24*, 2833.
- (15) Lu, J.; Ginis, V.; Lim, S. W. D.; Capasso, F. Helicity and Polarization Gradient Optical Trapping in Evanescent Fields. *Physical Review Letters* **2023**, *131*, 143803.

- (16) Sasaki, K.; Tsukima, M.; Masuhara, H. Three-dimensional potential analysis of radiation pressure exerted on a single microparticle. *Applied Physics Letters* **1997**, *71*, 37–39.
- (17) Barnes, W. L.; Dereux, A.; Ebbesen, T. W. Surface plasmon subwavelength optics. *Nature* **2003**, *424*, 824–830.
- (18) Zhang, Y.; Min, C.; Dou, X.; Wang, X.; Urbach, H. P.; Somekh, M. G.; Yuan, X. Plasmonic Tweezers: For Nanoscale Optical Trapping and Beyond. *Light: Science & Applications* **2021**, *10*, 59.
- (19) Kang, Z.; Chen, J.; Wu, S.-Y.; Chen, K.; Kong, S.-K.; Yong, K.-T.; Ho, H.-P. Trapping and assembling of particles and live cells on large-scale random gold nano-island substrates. *Scientific reports* **2015**, *5*, 9978.
- (20) Kotsifaki, D. G.; Chormaic, S. N. Plasmonic optical tweezers based on nanostructures: fundamentals, advances and prospects. *Nanophotonics* **2019**, *8*, 1227–1245.
- (21) Juan, M. L.; Righini, M.; Quidant, R. Plasmon nano-optical tweezers. *Nature Photonics* **2011**, *5*, 349–356.
- (22) Quidant, R.; Girard, C. Surface-plasmon-based optical manipulation. *Laser & Photonics Reviews* **2008**, *2*, 47–57.
- (23) Patra, P. P.; Chikkaraddy, R.; Tripathi, R. P.; Dasgupta, A.; Kumar, G. P. Plasmo-fluidic single-molecule surface-enhanced Raman scattering from dynamic assembly of plasmonic nanoparticles. *Nature Communications* **2014**, *5*, 4357.
- (24) Patra, P. P.; Chikkaraddy, R.; Thampi, S.; Tripathi, R. P.; Kumar, G. P. Large-scale dynamic assembly of metal nanostructures in plasmofluidic field. *Faraday discussions* **2016**, *186*, 95–106.

- (25) Cuche, A.; Canaguier-Durand, A.; Devaux, E.; Hutchison, J.; Genet, C.; Ebbesen, T. Sorting nanoparticles with intertwined plasmonic and thermo-hydrodynamical forces. *Nano Letters* **2013**, *13*, 4230–4235.
- (26) Sharma, V.; Tiwari, S.; Paul, D.; Sahu, R.; Chikkadi, V.; Kumar, G. P. Optothermal pulling, trapping, and assembly of colloids using nanowire plasmons. *Soft Matter* **2021**, *17*, 10903–10909.
- (27) Garcés-Chávez, V.; Quidant, R.; Reece, P.; Badenes, G.; Torner, L.; Dholakia, K. Extended organization of colloidal microparticles by surface plasmon polariton excitation. *Physical Review B* **2006**, *73*, 085417.
- (28) Volpe, G.; Quidant, R.; Badenes, G.; Petrov, D. Surface plasmon radiation forces. *Physical Review Letters* **2006**, *96*, 238101.
- (29) Kotsifaki, D. G.; Chormaic, S. N. The Role of Temperature-Induced Effects Generated by Plasmonic Nanostructures on Particle Delivery and Manipulation: A Review. *Nanophotonics* **2022**, *11*, 2199–2218.
- (30) Chen, Z.; Li, J.; Zheng, Y. Heat-mediated optical manipulation. *Chemical Reviews* **2021**, *122*, 3122–3179.
- (31) Kollipara, P. S.; Chen, Z.; Zheng, Y. Optical manipulation heats up: present and future of optothermal manipulation. *ACS Nano* **2023**, *17*, 7051–7063.
- (32) Kotnala, A.; Kollipara, P. S.; Li, J.; Zheng, Y. Overcoming diffusion-limited trapping in nanoaperture tweezers using opto-thermal-induced flow. *Nano Letters* **2019**, *20*, 768–779.
- (33) Sharma, V.; Paul, D.; Chaubey, S. K.; Tiwari, S.; Kumar, G. P. Large-scale optothermal assembly of colloids mediated by a gold microplate. *Journal of Physics: Condensed Matter* **2020**, *32*, 324002.

- (34) Peng, X.; Chen, Z.; Kollipara, P. S.; Liu, Y.; Fang, J.; Lin, L.; Zheng, Y. Opto-thermoelectric microswimmers. *Light: Science & Applications* **2020**, *9*, 141.
- (35) Shukla, A.; Tiwari, S.; Majumder, A.; Saha, K.; Kumar, G. V. P. Opto-Thermoelectric Trapping of Fluorescent Nanodiamonds on Plasmonic Nanostructures. *Optics Letters* **2023**, *48*, 2937–2940.
- (36) Wang, X.; Yuan, Y.; Xie, X.; Zhang, Y.; Min, C.; Yuan, X. Graphene-Based Opto-Thermoelectric Tweezers. *Advanced Materials* **2022**, *34*, 2107691.
- (37) Liu, Y.; Lin, L.; Bangalore Rajeeva, B.; Jarrett, J. W.; Li, X.; Peng, X.; Kollipara, P.; Yao, K.; Akinwande, D.; Dunn, A. K.; Zheng, Y. Nanoradiator-Mediated Deterministic Opto-Thermoelectric Manipulation. *ACS Nano* **2018**, *12*, 10383–10392.
- (38) Li, J.; Zheng, Y. Optothermally Assembled Nanostructures. *Accounts of Materials Research* **2021**, *2*, 352–363.
- (39) Kotnala, A.; Kollipara, P. S.; Zheng, Y. Opto-Thermoelectric Speckle Tweezers. *Nanophotonics* **2020**, *9*, 927–933.
- (40) Kollipara, P. S.; Lin, L.; Zheng, Y. Thermo-Electro-Mechanics at Individual Particles in Complex Colloidal Systems. *The Journal of Physical Chemistry C* **2019**, *123*, 21639–21644.
- (41) Maier, S. A.; others *Plasmonics: fundamentals and applications*; Springer, 2007; Vol. 1.
- (42) Baffou, G. *Thermoplasmonics: Heating Metal Nanoparticles Using Light*; Cambridge University Press, 2017.
- (43) Wang, K.; Schonbrun, E.; Crozier, K. B. Propulsion of gold nanoparticles with surface plasmon polaritons: evidence of enhanced optical force from near-field coupling between gold particle and gold film. *Nano Letters* **2009**, *9*, 2623–2629.

- (44) Bregulla, A. P.; Würger, A.; Günther, K.; Mertig, M.; Cichos, F. Thermo-osmotic flow in thin films. *Physical Review Letters* **2016**, *116*, 188303.
- (45) Fränzl, M.; Cichos, F. Hydrodynamic manipulation of nano-objects by optically induced thermo-osmotic flows. *Nature communications* **2022**, *13*, 656.
- (46) Duhr, S.; Braun, D. Why Molecules Move along a Temperature Gradient. *Proceedings of the National Academy of Sciences* **2006**, *103*, 19678–19682.
- (47) Quidant, R.; Zelenina, A.; Nieto-Vesperinas, M. Optical manipulation of plasmonic nanoparticles. *Applied Physics A* **2007**, *89*, 233–239.
- (48) Min, C.; Shen, Z.; Shen, J.; Zhang, Y.; Fang, H.; Yuan, G.; Du, L.; Zhu, S.; Lei, T.; Yuan, X. Focused plasmonic trapping of metallic particles. *Nature Communications* **2013**, *4*, 2891.
- (49) Jones, P. H.; Maragò, O. M.; Volpe, G. *Optical Tweezers: Principles and Applications*; Cambridge University Press, 2015.
- (50) Xu, Z.; Song, W.; Crozier, K. B. Direct particle tracking observation and Brownian dynamics simulations of a single nanoparticle optically trapped by a plasmonic nanoaperture. *ACS Photonics* **2018**, *5*, 2850–2859.
- (51) Chand, R.; Rani, C. E.; Paul, D.; Kumar, G. P. Emergence of Directional Rotation in an Optothermally Activated Colloidal System. *ACS Photonics* **2023**, *10*, 4006–4013.
- (52) Lin, L.; Wang, M.; Peng, X.; Lissek, E. N.; Mao, Z.; Scarabelli, L.; Adkins, E.; Coskun, S.; Unalan, H. E.; Korgel, B. A.; others Opto-thermoelectric nanotweezers. *Nature Photonics* **2018**, *12*, 195–201.
- (53) Lin, L.; Peng, X.; Wang, M.; Scarabelli, L.; Mao, Z.; Liz-Marzán, L. M.; Becker, M. F.; Zheng, Y. Light-directed reversible assembly of plasmonic nanoparticles using plasmon-enhanced thermophoresis. *ACS Nano* **2016**, *10*, 9659–9668.

- (54) Ohsawa, K.; Murata, M.; Ohshima, H. Zeta potential and surface charge density of polystyrene-latex; comparison with synaptic vesicle and brush border membrane vesicle. *Colloid and Polymer Science* **1986**, *264*, 1005–1009.
- (55) Brenner, H. The slow motion of a sphere through a viscous fluid towards a plane surface. *Chemical Engineering Science* **1961**, *16*, 242–251.
- (56) Tiwari, S.; Khandelwal, U.; Sharma, V.; Kumar, G. P. Single molecule surface enhanced Raman scattering in a single gold nanoparticle-driven thermoplasmonic tweezer. *The Journal of Physical Chemistry Letters* **2021**, *12*, 11910–11918.
- (57) Trivedi, M.; Saxena, D.; Ng, W. K.; Sapienza, R.; Volpe, G. Self-organized lasers from reconfigurable colloidal assemblies. *Nature Physics* **2022**, *18*, 939–944.

TOC Graphic

